JACS
JOURNAL OF THE AMERICAN CHEMICAL SOCIETY

Article

pubs.acs.org/JACS

Spontaneous Binding of Molecular Oxygen at the Q_o-Site of the bc_1 Complex Could Stimulate Superoxide Formation

Peter Husen* and Ilia A. Solov'yov*

Department of Physics, Chemistry and Pharmacy, University of Southern Denmark, Odense 5230, Denmark

Supporting Information

ABSTRACT: A key part of the respiratory and photosynthetic pathways is the bc_1 protein complex embedded in the inner membrane of mitochondria and the plasma membrane of photosynthetic bacteria. The protein complex pumps protons across the membrane to maintain an electrostatic potential, which is in turn used to drive ATP synthesis. This molecular machinery, however, is suspected to be a source of superoxide, which is toxic to the cell, even in minuscular quantities, and believed to be a factor in aging. Through molecular dynamics simulations, we investigate here the migration of molecular oxygen in the bc_1 complex in order to identify possible reaction sites that could lead to superoxide formation. It is found, in particular, that oxygen penetrates spontaneously the Q_o binding site of the bc_1 complex in the presence of an intermediate semiquinone radical, thus making the Q_o-site a strong candidate for being a center of superoxide production.

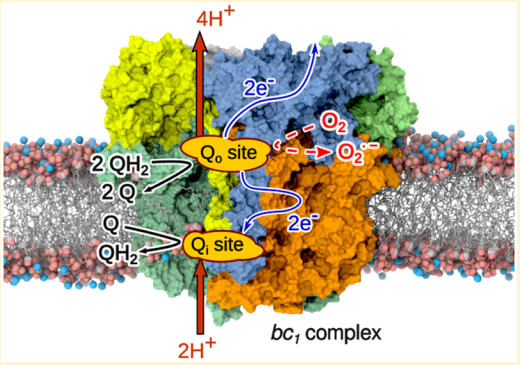

INTRODUCTION

The bc_1 protein complex[1,2] is found in the inner mitochondrial membrane in eukaryotes as well as the plasma membrane of photosynthetically active bacteria. It plays a central role in the metabolic pathway, where it is responsible for maintaining an electrostatic potential across the membrane, which is in turn used to drive ATP synthesis. The protein complex effectively pumps protons across the membrane through a series of redox processes between the complex and substrate ubiquinol (QH_2) and ubiquinone (Q) in the membrane, as featured in Figure 1.

The bc_1 complex operates through a reaction cycle referred to as the Q-cycle,[3] in which two QH_2 from the membrane are oxidized to Q, yielding 4 protons to the positive side of the membrane, while one Q is reduced to QH_2 with the uptake of 2 protons from the negative side, as illustrated schematically in Figure 1a.[3,4] The reaction cycle is mediated through internal electron transfers between charge centers in the protein complex.[4,5]

The bc_1 complex has two binding sites for the substrates: the Q_o-site near the positive side of the membrane, where QH_2 binds and is oxidized to Q, and the Q_i-site near the negative side, where Q binds and is reduced to QH_2. Both substrate binding sites are marked in Figure 1. Upon QH_2 oxidation, one electron from that molecule is transferred to the Q_i-site of the bc_1 complex to reduce a Q molecule bound there. Another electron from the QH_2 leaves the protein complex through a cytochrome *c* cofactor acting as electron carrier.[6]

The bc_1 complex is a dimer with each monomer consisting of three subunits, denoted in Figure 1b as cytochrome *b* (cyt *b*), cytochrome c_1 (cyt c_1) and the iron–sulfur protein (ISP).[1,7,8] Each subunit contains prosthetic groups, which are involved in

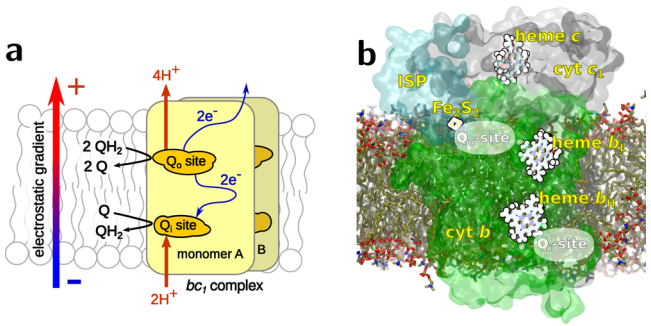

Figure 1. Charge transfer reactions in the cytochrome bc_1 complex and its constituent blocks. (a) Schematic drawing of the functioning of the bc_1 protein complex. During a complete reaction cycle, two quinols (QH_2) are oxidized to quinone (Q) at the Q_o binding site, while one quinone molecule is reduced to quinol at the Q_i-site. Protons are thus effectively transported from the negative to the positive side of the membrane, maintaining the electrostatic gradient. The reaction cycle is repeated in both monomers of the bc_1 complex, here denoted as monomers A and B. (b) A cross section of the membrane embedded bc_1 complex with the subunits (ISP, cyt c_1, cyt *b*) and prosthetic groups (Fe_2S_2, heme *c*, heme b_L, heme b_H) indicated for one monomer of the complex.

driving the functioning of the bc_1 complex: the cyt *b* subunit has two heme *b* groups (heme b_H and heme b_L), while the cyt c_1 subunit contains a heme *c* group, and the ISP holds an iron–sulfur cluster (Fe_2S_2) coordinated by two cysteine and two histidine residues of the protein.[1,9,10] The iron–sulfur cluster is

Received: May 11, 2016
Published: July 22, 2016

DOI: 10.1021/jacs.6b04849
J. Am. Chem. Soc. 2016, 138, 12150–12158

located at the Q_o-site with a covalently bound histidine residue of the ISP (H156 in case of *Rhodbacter capsulatus* structure[11]) to form a hydrogen bond with the QH_2 as it docks at the binding site.[5] At the Q_i-site, the Q molecule docks next to the heme b_H of the cytochrome *b* subunit.

A structure of the bc_1 complex with the QH_2 and Q substrates embedded at the binding sites has not been obtained from crystallography due to the metastable nature of the reaction complex.[11,12] However, a previous study[5] was able to computationally identify the precise binding motifs of the substrates inside the bc_1 complex starting from the crystal structure with the inhibitors stigmatelin and antimycin present at the binding sites. The present investigation builds upon the structure of the bc_1 complex from *Rhodobacter capsulatus* with the bound substrates obtained in that earlier investigation.

At intermediate stages of the Q-cycle, the substrates within the bc_1 complex exist as radicals, leading to the risk of rare stray reactions resulting in formation of byproduct radical species such as reactive and mobile superoxide ($O_2^{\bullet-}$),[13−18] which is highly toxic and may damage or even kill a cell if present in minimal concentrations.[19,20] Such stray redox reactions are believed to play a role in aging[21−26] and are, therefore, fundamentally important.

The necessary conditions for superoxide production viability are a small separation distance between the oxygen molecule and a potential electron donor and a noticeable binding time of the molecule within the bc_1 complex. Since an O_2 molecule is virtually not detectable in a microscope, the computational study is essentially the only possibility in revealing its dynamics. The migration of O_2 molecules into the bc_1 complex is, therefore, studied here through molecular dynamics simulations.

An intermediate stage of the Q-cycle is considered, where quinol has been only partially oxidized, leaving a semiquinone radical at the Q_o-site. While the specific form (neutral or anion) of semiquinone formed at the Q_o-site is still debated, there is experimental evidence[27] for the existence of the semiquinone anion ($Q^{\bullet-}$) at the Q_o-site, and earlier computational quantum chemical studies[5] suggest that both protons rapidly dissociate after the first electron transfer from quinol, and the anionic form was thus chosen for the present investigation. Simulations demonstrate that for this stage of the Q-cycle, molecular oxygen gets close to several charge centers of the bc_1 complex and is particularly able to migrate into and bind inside the Q_o-site.

METHODS

To study oxygen migration, molecular dynamics (MD) simulations were performed for the bc_1 complex from *Rhodobacter capsulatus* (PDB ID: 1ZRT[11]) embedded in a lipid membrane with ubiquinone (Q) molecules present at the Q_i-sites and semiquinone anions ($Q^{\bullet-}$) present at the Q_o-sites. The system consisting of the protein complex embedded in a membrane patch was suspended in a water box of 197 Å × 177 Å × 142 Å size using the TIP3P water model[28] with a neutralizing NaCl salt concentration of 0.05 mol/L. Oxygen molecules (O_2) were initially added to the water phase, and several simulations were performed. The simulations were carried out using NAMD 2.10[29] employing the CHARMM 36 force field with CMAP corrections.[30]

Computational Model of the bc_1 Complex. The computational model of the bc_1 complex used in the present investigation is similar to the model used previously.[5] The only modification concerns the redox state of the substrate bound at the Q_o-site. Here, it is considered oxidized to a semiquinone anion ($Q^{\bullet-}$), i.e., represents a QH_2 molecule, after it has donated an electron to the Fe_2S_2 cluster and both protons have dissociated. The protons are considered to be transferred to the H156 residue of the ISP and to the E295 residue of cyt *b* as suggested earlier.[5,31]

Force field parameters and partial charges for the heme groups of the bc_1 complex and the quinones originate from previous studies.[32,33] The parametrization of QH_2 and the Fe_2S_2 cluster from these sources was modified to construct the $Q^{\bullet-}$ model used in the present investigation; a negative charge was moved from the quinol headgroup to the Fe_2S_2 cluster, and the two protons from the QH_2 were moved to the H156 residue of the ISP and the E295 residue of cyt *b*, leaving them in a protonated state. Quantum chemical calculations were performed to identify the partial charges of the modified residues at the Q_o-site, while the CHARMM36 standard force field parameters were used for all other amino acid residues.

The Gaussian 09[34] quantum chemical software package was used for calculation of electrostatic potential (ESP) fitted charges for the $Q^{\bullet-}$ headgroup and the nearby amino acids from the protein complex using the B3LYP/6-311G(d) model chemistry.[35] The 6-311G(d) basis set was used specifically to ensure proper parametrization of the Fe_2S_2 atoms as also done previously.[5,36−43] A molecular cluster selection of 76 atoms, consisting of the $Q^{\bullet-}$ headgroup and the Fe_2S_2 cluster along with its coordinating amino acid residues (C133, C153, H135 and H156 of the ISP) was extracted from the full system and used for the quantum chemical calculations. The C_α atoms of C133, C153, H135 and H156, together with the backbone atoms of the amino acids as well as the $Q^{\bullet-}$ tail were replaced with methyl groups in the obtained cluster model. First, the geometry of the molecular cluster was structurally optimized, and then electrostatic potential (ESP) fitting was used to assign charges to individual atoms. Finally, the charges were rearranged slightly to impose hydrogen symmetries, which dictate equal charge of hydrogens of the same heavy atom and to assign integer charges to the entire $Q^{\bullet-}$ headgroup and the fragment consisting of the Fe_2S_2 cluster and its coordinating amino acid residues. These modifications were applied in order to assign atomic partial charges in line with the parametrization strategy of the standard CHARMM force fields employed in MD simulations. The obtained charges are provided in the Supporting Information (SI).

The lipid bilayer was taken consistent with the earlier study,[5] where a mixture of phosphatidylcholines (PC 18:2/18:2), phosphatidylethanolamines (PE 18:2/18:2) and cardiolipins (CL 18:2/18:2/18:2) was used with a total of 102 CL, 406 PC and 342 PE lipids in the membrane patch. Standard CHARMM36 provides parameters for PC and PE lipids, but not for CL. Therefore, parameters for the headgroup of this lipid type were taken from a previous investigation,[44] while CHARMM36 parameters for the lipid tails were used.

Adding Molecular Oxygen into the System. O_2 molecules were added to the system by randomly substituting a number of bulk water molecules with O_2. Two scenarios were considered: simulations with a high and low O_2 concentrations, see Table 1. In the case of a high oxygen concentration, a total of 165 oxygen molecules was added to the system, corresponding to oxygen concentration of ∼100 mmol/L in the bulk water before oxygen diffuses into the membrane and the bc_1 complex. This is about 2−3 orders of magnitude higher than physiological oxygen concentrations,[45] but a more realistic concentration would not have a single molecule inside the simulation box—hence, the exaggerated concentration is used to allow observations and even statistics of O_2 binding and unbinding events within the time scales available to atomistic MD simulations. In the case of low O_2 concentration, a single molecule was placed inside the simulation box, and a number of simulations were carried out to test for possible artifacts due to oxygen−oxygen interactions. The latter simulations are discussed in the SI. O_2 was modeled using the standard CHARMM36 force field.[30]

Langevin Dynamics Simulations. The dynamics of the membrane-embedded bc_1 complex was studied using Langevin dynamics. The integration time step of 2 fs was used, and the simulations were performed using periodic boundary conditions. A smooth cutoff of 12 Å was used for electrostatic and van der Waals interactions, and long-range electrostatic interactions were treated with the particle-mesh Ewald (PME) summation method.[46] The initial molecular structure used for the simulations was adopted from an

DOI: 10.1021/jacs.6b04849
J. Am. Chem. Soc. 2016, 138, 12150−12158

Table 1. bc_1 Protein Complex Simulations in the Presence of Oxygen Molecules[a]

	O_2 concentration	n_{O_2}	γ (1/ps)	simulation time (ns)	repetitions
a	high	165	1	50	1
			2	50	1
			4	50	1
			7	50	1
			10	50	1
b	high	165	5	370	2
c	low	1	5	30	6

[a]Three types of simulations were carried out in the present investigation. (a) The first five simulations vary the damping constant γ of the Langevin thermostat, eq 1, and are used to determine the physically correct value of γ that resembles the diffusive properties of O_2 in water as outlined in the SI. (b) Next, extended production simulations used to analyze the localization and binding time of oxygen molecules inside the bc_1 complex were carried out. The simulation was repeated twice. The simulations of category a and b were performed with an exaggerated number of O_2 molecules to improve O_2 binding statistics. (c) Finally, a single oxygen molecule was placed initially near the Q_o binding site, and 6 independent simulations were carried out for 30 ns each to probe the O_2 binding mechanism with only a single O_2 molecule being present in the bc_1 complex.

earlier investigation,[5] where it had been equilibrated for a total of 310 ns followed by a production simulation of 360 ns. After applying the small modifications at the Q_o-site in the present study, the system was equilibrated further for 3 ns with the backbone atoms of the bc_1 complex fixed and explicit constraints artificially added between residues of the protein and the substrate quinones and semiquinones to keep them in the binding sites. The equilibration was carried out using the Nosé-Anderson-Langevin piston pressure control with a piston oscillation period of 200 fs and a decay time of 50 fs to keep the system at atmospheric pressure, allowing the volume to fluctuate (NPT ensemble). After equilibration, all the constraints were released, and the production MD simulations were carried out in the NVT ensemble with a simulation box of size 197 Å × 177 Å × 142 Å.

The temperature was maintained at 310 K using the Langevin thermostat, which applies a viscous force to all heavy atoms in the system proportional to their velocity $\mathbf{v}$ and a random force, which follows a Gaussian distribution:[47,48]

$$\mathbf{F}_{\text{Langevin}} = -\gamma m\mathbf{v} + \sqrt{2\gamma m k_B T}\,\mathbf{R}(t) \quad (1)$$

Here, m is the mass of an atom, γ is the damping coefficient, k_B is the Boltzmann constant and T is the temperature. The random force $\mathbf{R}(t)$ is a delta-correlated Gaussian process. A value of the damping constant of γ = 5 ps^{-1} was generally used, as it was established from the benchmark simulations discussed below to correctly represent diffusion of oxygen in water.

A number of benchmark simulations were carried out to test the limitations of the computational model and simulation technique. First, simulations with different values γ were carried out, as indicated in Table 1a, to justify the use of the Langevin thermostat by measuring the effect of the Langevin damping coefficient γ on oxygen diffusion by varying the value of γ, see Table 1a. Then, additional benchmark simulations were dedicated to test for artifacts due to the artificially high oxygen concentration: Simulations of O_2 molecules in a water box, summarized in Table S1, were carried out with both high and low oxygen concentration to test if the artificially high concentration affects the diffusive properties of individual molecules, and a set of simulations of the bc_1 complex with a single O_2 molecule, see Table 1c, initially placed close to the Q_o binding site were carried out to test the dynamics of an O_2 molecule inside the bc_1 complex in the absence of other O_2 molecules. The results of these benchmark simulations are presented in the SI.

RESULTS

The present study deals to a large extend with the analysis of oxygen diffusion within the bc_1 complex as well as its exterior. The diffusive properties of oxygen in the MD model[49] presented here are, therefore, evaluated in the SI to ascertain a reasonable agreement with experimental observations.[50] Specifically, the dependence of the diffusion constant D of O_2 in water on the Langevin damping constant γ was measured and shown in Figure S1, and it was found that the commonly used value of γ = 5 ps^{-1} for MD simulations produces a reasonable agreement with experimentally obtained[50] values of D, and this value of γ was thus chosen for the simulations in the present investigation. It was also found that the exaggerated oxygen concentration does not significantly affect the diffusion constant of individual O_2 molecules due to, e.g., clustering together.

In the following, the general localization of oxygen in the bc_1 complex is first discussed—in particular at the Q_o binding site and near the heme groups involved in electron transfer processes, where the presence of oxygen poses a high risk of superoxide production. Then, the specific path of entry into the Q_o-site is revealed in more detail, and finally the time scales and rates of O_2 migration and binding in the bc_1 complex and the relation to superoxide production rates are discussed.

Oxygen Localization in the bc_1 Complex. Once molecular oxygen is added to the bulk water phase in the simulation box containing the membrane embedded bc_1 complex, the molecules rapidly diffuse and partition preferentially into the membrane. This is consistent with oxygen molecules being nonpolar and thus preferring the hydrophobic environment inside the membrane.[51] Figure 2 shows the z-profile of the O_2 concentration averaged over the entire MD trajectory of 370 ns, assuming the high oxygen concentration in the simulation box, see Table 1b. This concentration profile is calculated as a histogram of z coordinates of oxygen molecules sampled over the trajectory. The concentration of O_2 molecules in a z-slice of the simulation box of width Δz is defined as

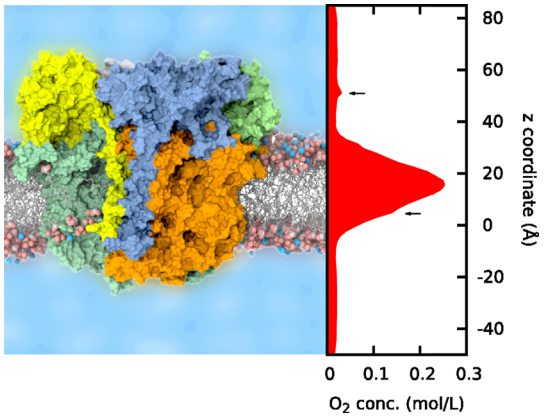

Figure 2. Oxygen concentration in the bc_1 complex. Average concentration of oxygen molecules observed in the simulations, computed as a function of the z coordinate, i.e., a direction perpendicular to the membrane using eq 2. Some irregularities are indicated with horizontal arrow markers.

DOI: 10.1021/jacs.6b04849
J. Am. Chem. Soc. 2016, 138, 12150−12158

$$c_{O_2}(z) = \frac{\langle N_{O_2}(z)\rangle_{\text{trajectory}}}{N_A l_x l_y \Delta z} \quad (2)$$

where $N_{O_2}(z)$ is the number of O_2 molecules in the slice of the simulation box centered at the z-coordinate, N_A is the Avogadro constant, l_x and l_y are the dimensions of the simulation box, and $\Delta z = 1.78$ Å is the histogram bin size on the z-axis used to slice the simulation box. The oxygen concentration away from the membrane and the bc_1 complex, which corresponds to the z-values of $z \leq -20$ Å and $z \geq 60$ Å, is 20.9 mmol/L as indicated in Table S2 in the SI, being the concentration of oxygen in water effectively modeled by the simulations.

Some other features can be observed in this histogram in Figure 2 at around $z = 5$ Å and $z = 50$ Å, where small bumps in the oxygen concentration manifest. These features are indicated by arrows in Figure 2 and correspond to increased concentrations of O_2 within regions of the protein that show an increased affinity to molecular oxygen.

O_2 molecules are also found to readily diffuse into parts of the bc_1 complex. Figure 3 shows trajectory averaged oxygen density isosurfaces in one monomer of the bc_1 complex, essentially indicating the sites with frequent observations of molecular oxygen. As seen in Figure 3a, there is a region where oxygen molecules were frequently observed located fairly close to the Q_o-site, near the headgroup of the $Q^{\bullet-}$ as well as the Fe_2S_2 cluster and the Y302 residue of the cyt b subunit. In the simulated trajectories, it is observed that molecular oxygen tends to bind inside the Q_o-site and stay there for an extended time—typically on the order of 10−30 ns as seen in Figure 4a. Occasionally, the O_2 molecule moves close to the $Q^{\bullet-}$ headgroup, which could lead to oxidation of the oxygen molecule to superoxide, strongly suggesting that the Q_o-site with a bound $Q^{\bullet-}$ anion could be a major source of superoxide ($O_2^{\bullet-}$) production in the bc_1 complex.

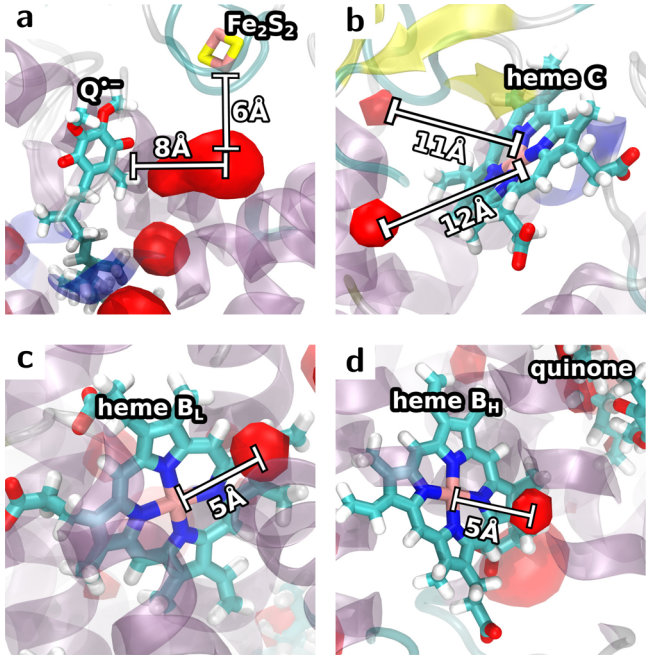

Figure 3. Localization of molecular oxygen at various sites of the bc_1 protein complex. The red surfaces indicate isosurfaces of the density map of O_2 in the simulation box averaged over the entire trajectory of 369 ns, i.e., the surfaces indicate regions where oxygen molecules are often observed. (a) Localization of oxygen at the Q_o-site of the bc_1 complex. The large region with indicated distances is the binding pocket, where an oxygen molecule tends to stay for an extended time, see Figure 4. The isovalue of 2.2 nm^{-3} was used to determine the O_2 localization area. (b−d) Oxygen localization at hemes c, b_L and b_H, respectively. Lower isovalues of 0.2 nm^{-3}, 1.5 nm^{-3} and 0.8 nm^{-3}, respectively, were used to compute the isosurfaces in these cases, as compared to the O_2 localization at the Q_o-site, i.e., oxygen is observed less frequently at the heme groups. See also Figure 4a.

Molecular oxygen was also observed near the heme groups of the bc_1 complex, particularly hemes b_L and b_H, see Figure 3c,d, although to a lesser extend than at the Q_o-site. While oxygen spends less time at the heme groups, see Figure 4, these could also be considered as potential electron donors for superoxide production. In particular, the binding of O_2 close to the heme group would have the advantage (from a superoxide production point of view) that the resulting superoxide would likely be able to diffuse away from the protein complex more rapidly than if produced at the Q_o-site, where the superoxide would be formed deep inside the cavity of the binding site.

Figure 4 shows the distance from the nearest O_2 molecule to the centers of the iron-containing prosthetic groups of the bc_1 complex, i.e., the Fe_2S_2 cluster and the heme groups. Also shown is the percentage of the total simulation time an O_2 molecule is within a threshold distance of 10 Å. In case of the Fe_2S_2 cluster (Figure 4a), this percentage provides a measure of the relative time an oxygen molecule is bound at the Q_o-site of the bc_1 complex, as the bound state represents the closest encounter of the O_2 molecules with Fe_2S_2. The tendency of O_2 to stay bound for extended periods (tens of nanoseconds) can be seen from the time dependence of the O_2−Fe_2S_2 distance plotted in Figure 4a. From inspecting the trajectories, it is observed that only a single oxygen molecule at a time can occupy the Q_o-site.

O_2 Path into the bc_1 Complex. To study how molecular oxygen migrates into the Q_o-site of the bc_1 complex in detail, a set of 21 trajectories of individual oxygen molecules entering or leaving the binding site were extracted from the high O_2 concentration simulation, see Table. 1b. These trajectories were then averaged and resampled to produce a rough path, shown in Figure 5b, of oxygen molecules entering the Q_o-site of the bc_1 complex.

In the majority of cases, the oxygen molecules enter the protein complex from inside the membrane between the cyt c protein and the part of the ISP that traverses the membrane as sketched in Figure 5a. The molecules then follow a path along the tail region of the $Q^{\bullet-}$ through a cavity leading to the Q_o-site as shown in the averaged O_2 trajectory in Figure 5b. Here, an oxygen molecule occasionally binds in the region between Y302 of the cyt b subunit and the Fe_2S_2 cluster, where it stays for periods of typically 10−30 ns, see Figure 4. In simulations of just a single O_2 molecule in the simulation box placed initially near the Q_o-site of the bc_1 complex, see Table 1c, the O_2 molecule is found to bind at the Q_o-site in one out of six cases and leaves the cavity following the same path as described above for the high oxygen concentration simulations after staying in the bound position for 36 ns, indicating that the mechanism is not dependent on effects due to the artificially high oxygen concentration. The single O_2 molecule simulations are discussed in more detail in the SI, and the trajectory of the single O_2 molecule leaving the Q_o-site is shown in Figure S3.

Watching the individual trajectories, the O_2 molecules are found to jump between locally confined positions on their way through the narrow cavity. This observation is in line with

DOI: 10.1021/jacs.6b04849
J. Am. Chem. Soc. 2016, 138, 12150−12158

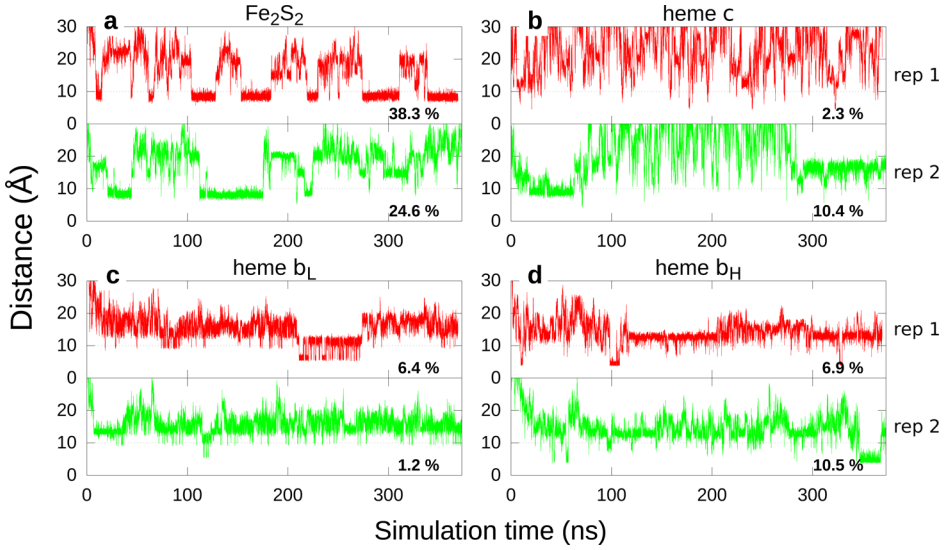

Figure 4. O_2 binding characterization within the bc_1 complex. Distance from the nearest O_2 molecule to the various parts of the bc_1 complex for the case of high oxygen concentration, see Table 1b, as a function of the simulation time. The red and green curves represent results of two repetitive simulations. The percentages indicate the relative duration of an O_2 molecule being within 10 Å of the Q_o-site (a), heme *c* (b), heme b_L (c), or heme b_H (d). (a) The distance of O_2 to the iron−sulfur cluster at the Q_o-site of the bc_1 complex. Once an O_2 molecule emerges closer than 10 Å away from the Fe_2S_2 cluster, it appears inside the binding pocket of the Q_o-site, as illustrated in Figure 5 and Figure 3a, where it tends to stay for an extended duration. (b−d) The distances between the nearest O_2 molecule and the centers of the hemes *c*, b_L and b_H, respectively.

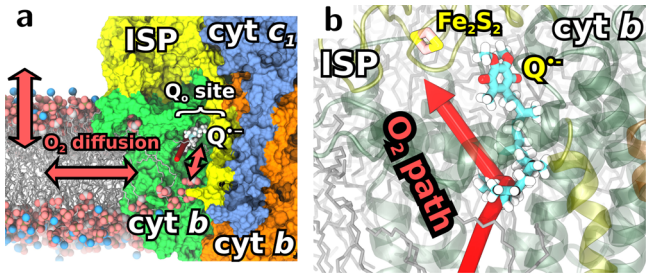

Figure 5. Migration path of oxygen molecules into the Q_o-site of the bc_1 complex. The oxygen molecules readily diffuse from the water phase into the membrane and from there into the protein complex. Inside the complex, the O_2 molecules migrate through the same cavity as the QH_2 substrate diffuses into the Q_o-site along the path indicated by a thick red arrow. This path was obtained by averaging a set of trajectories for individual O_2 molecules entering or leaving the binding site. These individual O_2 molecule trajectories were extracted from the high O_2 concentration simulation, see Table 1b. (a) Oxygen molecules enter the bc_1 complex from inside the membrane. (b) The O_2 trajectory inside the complex leading to the Q_o-site.

earlier findings[52] that small hydrophobic molecules migrate through narrow channels with the help of random fluctuations of the protein conformation, which occasionally open up bottlenecks of the pathway.

The fact that O_2 migrates into the Q_o-site along the same path as the quinol substrate from the membrane suggests that mutations of residues near the Q_o-site that might influence the tendency of oxygen to bind inside the Q_o-site would likely also affect the ability of QH_2 to bind there. However, this possibility is interesting to be investigated separately in greater detail.

Time Scales of Oxygen Trapping at the Q_o-Site. The performed MD simulations allow to make a first step toward estimating the relevant time scales of superoxide production in the bc_1 complex and in particular study the times of oxygen trapping at the reactive sites of the bc_1 complex. The time scales for the two major steps of the migration of O_2 molecules will be estimated separately: (i) the diffusion time of O_2 from the membrane into the bc_1 complex and then (ii) the time of further O_2 migration inside the complex into the Q_o-site. However, since O_2 molecules can freely migrate backward at any part of the process, until trapped at the Q_o-site, these time scales can not simply be added. Instead, an estimate is provided for total time of the combined process, as measured directly from the simulations.

First, the lateral diffusion of oxygen molecules in the membrane is considered. The lateral diffusion coefficient of O_2 molecules in the membrane can be determined from the performed simulations using a 2-dimensional variant of the analysis of diffusive properties of O_2 in the SI. Specifically, normal distributions, cf. eq S1, are fit to the distributions of x and y components of displacement vectors of O_2 molecules inside the membrane. This analysis delivers a lateral diffusion coefficient of $D_{xy} \simeq 0.15$ Å^2/ps.

As the solution of the two-dimensional diffusion equation depends strongly on the surface geometry, a specific exemplary membrane with embedded bc_1 complexes is considered—specifically the chromatophore vesicle found in the purple bacteria *Rhodobacter sphaeroides*, which contains $N_{bc_1} = 4$ bc_1 complexes and has a diameter of around R = 600 Å.[53] A mathematical model that describes diffusion of a randomly moving particle on a spherical surface with a distribution of N small circular traps of equal radius r was extensively discussed in an earlier investigation[54] and could be applied now to estimate the time needed for an oxygen molecule in the chromatophore membrane to hit a random bc_1 complex. The model suggests to estimate the mean first passage time of the diffusing particle hitting a trap, i.e., a bc_1 complex, as

$$\langle \tau \rangle \sim \frac{4\pi R^2}{D}\left[\frac{2}{N}\log\frac{R}{r} - \left(\frac{\log N}{N} + \frac{l_1}{N} + O(N^{-2})\right)\right] \quad (3)$$

DOI: 10.1021/jacs.6b04849
J. Am. Chem. Soc. 2016, 138, 12150−12158

where D is the lateral diffusion coefficient on the surface and l_1 = 0.10569 is a numerically determined constant. Eq 3 represents the solution of an optimization problem that positions the traps on the surface to minimize the mean first passage time. The lateral size of the bc_1 complex is readily taken as the size of its bounding box, which extents in both the x and y directions by roughly 100 Å. This value is, therefore, put to be the diameter of a circular target in the membrane, i.e., having a radius of r = 50 Å. Putting in all the parameters yields a value of

$$\langle \tau \rangle \simeq 4\ \mu s \tag{4}$$

of the time it takes for a randomly placed O_2 molecule in the exemplary chromatophore membrane to reach any bc_1 complex.

From the point of view of a specific bc_1 complex, the average time between trapping O_2 molecules can then be estimated by knowing the average number of O_2 molecules in the examplary membrane. In the simulations, the concentration of molecular oxygen in the membrane could be estimated by averaging the part of the concentration profile shown in Figure 2 within the membrane, which corresponds to the interval 0 Å < z < 35 Å. This yields a concentration of 160 mmol/L, i.e., a value about 8 times greater than the concentration of O_2 in water, as follows also from Table S2 in the SI. The more realistic concentration c_{O_2/H_2O} = 100 μmol/L[45] of O_2 in water lead to the concentration of O_2 inside the membrane being equal to $c_{O_2/mem} \simeq 8c_{O_2/H_2O}$ = 800 μmol/L. Taking the thickness of the membrane equal to Δz = 35 Å, the corresponding lateral density of oxygen molecules is found as

$$\rho_{O_2/mem} = N_A \Delta z c_{O_2/mem} = 1.7 \cdot 10^{-5}\ \text{Å}^{-2} \tag{5}$$

This leads to an average of $N_{O_2} = 4\pi R^2\ \rho_{O_2/mem}$ = 19 O_2 molecules in the exemplary chromatophore membrane, so the estimate in eq 4 can be rescaled to

$$\langle \tau_1 \rangle = \frac{N_{bc_1}}{N_{O_2}} \langle \tau \rangle = 0.8\ \mu s \simeq 1\ \mu s \tag{6}$$

for *any* O_2 molecule reaching a *specific* bc_1 complex—i.e., a rate of one event per bc_1 complex per microsecond.

The time required for migration of an O_2 molecule within the bc_1 complex to the Q_o-site can be estimated directly from the performed MD simulations. In the high oxygen concentration simulations (Table 1b), an average number of N_{O_2/bc_1} = 38 O_2 molecules were observed simultaneously within the bc_1 complex and a circular surrounding membrane patch of 50 Å radius. Figure 4a shows that an O_2 molecule is bound a fraction of $x_{O_2} \simeq$ 30% of the simulation time, and roughly N_{bind} = 10 independent binding events are observed during the entire Δt = 370 ns long simulation, so the average time τ_{vac}, the Q_o-site is vacant in the simulations, before an O_2 molecule is bound is

$$\tau_{vac} = \frac{(1 - x_{O_2})\Delta t}{N_{bind}} \simeq 26\ \text{ns} \tag{7}$$

Assuming the average vacant time is inversely proportional to the oxygen concentration, the migration time τ_{bc_1} of a single O_2 molecule within the bc_1 complex to the Q_o-site can thus be estimated by rescaling the vacant time by the number of O_2 molecules in bc_1 complex in the simulations, i.e., essentially rescaling to a concentration that has a single O_2 molecule on average within the complex:

$$\tau_{bc_1} = N_{O_2/bc_1} \tau_{vac} \simeq 1\ \mu\text{s/event} \tag{8}$$

However, the bc_1 complex is not quite an absorbing target—most O_2 molecules reaching a bc_1 complex from the membrane will likely diffuse away again and not reach the Q_o-site, as follows from the supporting simulations discussed in the SI, where an O_2 molecule was placed close to the Q_o-site. The time interval in eq 8 is thus essentially distributed over multiple "attempts", i.e., events where an O_2 molecule has reached a bc_1 complex. A simple way to estimate the total time for any O_2 molecule to diffuse to a particular bc_1 complex, migrate within the complex and bind at the Q_o-site is to rescale the value in eq 7 instead to a realistic concentration of O_2 molecules in water. As the simulated oxygen concentration in the water phase is roughly 200 times (see Table S2 in the SI) greater than the more realistic value of 100 μmol/L,[45] the total time before an oxygen molecule binds at the Q_o-site of a particular bc_1 complex can be estimated as

$$\tau_{bind} = 200 \times \tau_{vac} \simeq 5\ \mu\text{s/event} \tag{9}$$

i.e., corresponding to an O_2 binding rate of $k_{bind} \simeq 0.2\ \mu s^{-1}$. Note that this estimate is obtained directly from the simulations and is the rate per bc_1 complex regardless of the particular arrangement or concentration of bc_1 complexes in the membrane. Compared to eq 6, the estimate in eq 9 includes both diffusion to the bc_1 complex and migration to the Q_o-site. A direct comparison of the two estimates suggests that roughly one in five O_2 molecules that reach a bc_1 complex will also bind at the Q_o-site.

To estimate the rate of superoxide production due to electron transfer at the Q_o-site with bound $Q^{\bullet-}$ and O_2, additional unknown parameters need to be established. Assuming O_2 is bound at the Q_o-site only a small fraction of time at realistic oxygen concentrations, the rate of superoxide production per bc_1 complex, while $Q^{\bullet-}$ is bound at the Q_o-site, can be estimated as

$$k_{O_2^{\bullet-}} = k_{bind} \frac{k_{et}}{k_{et} + k_{unbind}} \tag{10}$$

where $k_{bind} = \tau_{bind}^{-1}$ is the oxygen binding rate at the Q_o-site, k_{et} is the intrinsic electron transfer rate, when both $Q^{\bullet-}$ and O_2 are bound at the Q_o-site and, finally, k_{unbind} is the average O_2 unbinding rate, which is taken as the inverse of the average O_2 residence time and assumed to be independent of the oxygen concentration:

$$k_{unbind} = \frac{N_{bind}}{x_{O_2} \Delta t} \simeq 0.1\ \text{ns}^{-1} \tag{11}$$

The fraction in eq 10 reflects the competition between the two processes that take the system out of the bound O_2 state: unbinding of O_2 from the Q_o-site or electron transfer to O_2 to form $O_2^{\bullet-}$. In the limiting regimes of very high ($k_{et} \gg k_{unbind}$) or very low ($k_{et} \ll k_{unbind}$) electron transfer rates, one then obtains:

$$k_{O_2^{\bullet-}} \simeq \begin{cases} 0.2\ \mu s^{-1} & \text{for high } e^- \text{ transfer rate} \\ 5 \cdot 10^4 \times k_{et} & \text{for low } e^- \text{ transfer rate} \end{cases} \tag{12}$$

To estimate the overall rate of $O_2^{\bullet-}$ production, one needs to take into account the lifetime of the $Q^{\bullet-}$ which releases its electron in a second electron transfer at the Q_o-site.[31] The

DOI: 10.1021/jacs.6b04849
J. Am. Chem. Soc. 2016, 138, 12150−12158

details of this second electron transfer at the Q_o-site oxidizing the $Q^{\bullet-}$ fully to Q are controversial,[55] and the $Q^{\bullet-}$ intermediate is generally believed to be relatively short-lived, before the second electron transfer to heme b_L occurs. The probability of finding a bc_1 complex in the $Q^{\bullet-}$ state is argued[55] to be on the order of $x_{Q^{\bullet-}} \simeq 4 \times 10^{-8}$, which leads to the overall superoxide production rate:

$$K_{O_2^{\bullet-}} = x_{Q^{\bullet-}} k_{O_2^{\bullet-}} \simeq \begin{cases} 8\ \mathrm{ms}^{-1} & \text{for high } e^- \text{ transfer rate} \\ 2\cdot 10^{-3} \times k_{et} & \text{for low } e^- \text{ transfer rate} \end{cases} \quad (13)$$

As the molecular environment at the Q_o-site is quite complex, it is not straightforward to estimate the rate of the putative electron transfer process to O_2. It is, therefore, imperative that a complete multiscale computational model of superoxide production at the Q_o-site of the bc_1 complex needs at least to be extended with quantum chemical calculations of possible electron transfer processes between the bc_1 complex, substrate molecules and O_2.

Experimental studies[56] of rat mitochondria find yields between 0.1 and 0.5 superoxide radicals per second per bc_1 complex under the presence of antimycin inhibiting the Q_i-site of the bc_1 complex, which stalls the Q cycle and favors the presence of semiquinone at the Q_o-site. This is about an order of magnitude higher than the maximum rate estimated in eq 13, but this difference could easily be explained by the inhibition by antimycin in the experimental study. On the other hand, in the same investigation,[56] a kinetic model is employed to find values specifically of the rate $k_{O_2^{\bullet-}}$ of reactions between semiquinone and O_2 ranging between 1 and 40 per second per bc_1 complex, when semiquinone is present at the Q_o-site. This is around 4 orders of magnitude higher than the estimate in eq 12 in case of high electron transfer rate. For eq 12 to produce a superoxide production rate of 40 s^{-1}, the unknown electron transfer rate would have to be as low as 0.2 μs^{-1}. However, it should be noted that the experimentally observed rates are rather indirectly obtained through fitting of a kinetic model and thus likely rather sensitive to the details of the model. For example, it does not differentiate between the neutral semiquinone ($QH^{\bullet}$) state and the semiquinone anion ($Q^{\bullet-}$).

CONCLUSION

The present work investigates the dynamics of molecular oxygen in the bc_1 complex as a first step toward a complete computational model of superoxide production in the bc_1 complex. For this reason, a model of the bc_1 complex from *Rhodobacter capsulatus* was established featuring semiquinone anions ($Q^{\bullet-}$) bound at the Q_o-sites, and MD simulations in the presence of molecular oxygen were carried out.

The computational results show that O_2 molecules diffuse spontaneously into the bc_1 complex and all the way into the Q_o-site, where QH_2 binds and is oxidized to an intermediate $Q^{\bullet-}$ before it gets fully oxidized to Q. Specifically, the O_2 molecules enter the bc_1 complex from the membrane and then find their way into the Q_o-site along the cavity housing the tail region of the bound semiquinone. The ability of oxygen molecules to reach the Q_o-site in the presence of the intermediate $Q^{\bullet-}$ is a necessary condition for superoxide production to occur at the Q_o-site through reduction of O_2 by the $Q^{\bullet-}$ radical, which is the mechanism proposed earlier.[13,17,57−59] The simulated O_2 trajectories further show that an oxygen molecule occasionally becomes trapped inside the Q_o-site next to the tyrosine Y302 residue (in *Rhodobacter capsulatus*) of the cyt *b* subunit, which puts it within 10 Å of the Fe_2S_2 cluster. Once trapped, it typically stays there for tens of nanoseconds, significantly increasing the probability of a redox reaction to occur.

However, oxygen molecules also occasionally get within 5 Å of the central iron atom of the hemes b_L and b_H, which are part of the electron transfer chain in the Q cycle of the bc_1 complex. Hence, these groups should also be considered as potential electron donors in the production of superoxide. While molecular oxygen is close to the heme groups a smaller fraction of the time, a superoxide molecule formed there would, on the other hand, diffuse much more easily away from the bc_1 complex, compared to a superoxide at the Q_o site, which needs to exit the deep cavity of the binding site.

The computational model of molecular oxygen in the system was justified through benchmark simulations aimed to investigate its limitations: In particular, (i) the diffusive properties of small molecules may not be well characterized when using the Langevin thermostat in MD simulations. However, it was found through simulations with varying values of the Langevin damping constant γ that the diffusion coefficient of oxygen in water obtained from simulations with a damping constant of $\gamma = 5\ \mathrm{ps}^{-1}$ was reasonably close to experimentally obtained values.[50] (ii) a greatly exaggerated concentration of oxygen was used in order to realistically obtain meaningful statistics of O_2 binding within the Q_o-site of the bc_1 complex. The artificially high concentration was justified by comparing the diffusive properties of O_2 molecules in simulations with the exaggerated concentration and those where a single O_2 molecule was placed in the simulation box.

Finally, the relevant time scales of O_2 diffusion and migration into the Q_o-site of the bc_1 complex were discussed, suggesting the time scale of around 1 μs for an O_2 molecule from the membrane to enter the bc_1 complex and 5 μs for an O_2 molecule to enter and bind at the Q_o-site. The estimates thus demonstrate that MD simulations of the O_2 binding process at biologically relevant O_2 concentrations is unrealistic. Further description of the multiscale process of superoxide formation involves establishing the probability of the $O_2 + e^- \rightarrow O_2^{\bullet-}$ reaction to occur and of superoxide leaving the bc_1 complex without reacting again with various parts of the protein complex. These studies are, however, also infeasible for the classical MD treatment and require input from quantum chemistry. Combining quantum chemical calculations and classical MD simulations into a truly multiscale description of the potential electron transfer processes at the Q_o-site or near the heme groups of the bc_1 complex is thus considered one of the most promising routes to describe precisely the origin of superoxide production inside the bc_1 complex.

ASSOCIATED CONTENT

Supporting Information

The Supporting Information is available free of charge on the ACS Publications website at DOI: 10.1021/jacs.6b04849.

Diffusive properties of molecular oxygen in the simulations and the dynamics of a single O_2 molecule in the bc_1 complex; partial charges at the Q_o-site of the bc_1 complex obtained through quantum chemical calculations in the form of a CHARMM topology file (PDF)

DOI: 10.1021/jacs.6b04849
J. Am. Chem. Soc. 2016, 138, 12150−12158

AUTHOR INFORMATION

Corresponding Authors

*phusen@sdu.dk

*ilia@sdu.dk

Notes

The authors declare no competing financial interest.

ACKNOWLEDGMENTS

The authors thank the Lundbeck Foundation and the Russian Science Foundation (Grant No. 14-12-00342) for financial support. Computational resources for the simulations were provided by the DeiC National HPC Center, SDU.

REFERENCES

(1) Crofts, A. R.; Berry, E. A. *Curr. Opin. Struct. Biol.* **1998**, *8*, 501−509.

(2) Mulkidjanian, A. Y. *Biochim. Biophys. Acta, Bioenerg.* **2005**, *1709*, 5−34.

(3) Mitchell, P. *FEBS Lett.* **1975**, *59*, 137−139.

(4) Cramer, W. A.; Hasan, S. S.; Yamashita, E. *Biochim. Biophys. Acta, Bioenerg.* **2011**, *1807*, 788−802.

(5) Barragan, A. M.; Crofts, A. R.; Schulten, K.; Solov'yov, I. A. *J. Phys. Chem. B* **2014**, *119*, 433−447.

(6) Sarewicz, M.; Osyczka, A. *Physiol. Rev.* **2015**, *95*, 219−243.

(7) Yang, X.; Trumpower, B. *J. Biol. Chem.* **1986**, *261*, 12282−12289.

(8) Degli Esposti, M.; De Vries, S.; Crimi, M.; Ghelli, A.; Patarnello, T.; Meyer, A. *Biochim. Biophys. Acta, Bioenerg.* **1993**, *1143*, 243−271.

(9) Rieske, J. S.; MacLennan, D. H.; Coleman, R. *Biochem. Biophys. Res. Commun.* **1964**, *15*, 338−344.

(10) Reedy, C. J.; Gibney, B. R. *Chem. Rev.* **2004**, *104*, 617−650.

(11) Berry, E. A.; Huang, L.-S.; Saechao, L. K.; Pon, N. G.; Valkova-Valchanova, M.; Daldal, F. *Photosynth. Res.* **2004**, *81*, 251−275.

(12) Esser, L.; Elberry, M.; Zhou, F.; Yu, C.-A.; Yu, L.; Xia, D. *J. Biol. Chem.* **2008**, *283*, 2846−2857.

(13) Dröse, S.; Brandt, U. *J. Biol. Chem.* **2008**, *283*, 21649−21654.

(14) Guillaud, F.; Dröse, S.; Kowald, A.; Brandt, U.; Klipp, E. *Biochim. Biophys. Acta, Bioenerg.* **2014**, *1837*, 1643−1652.

(15) Rottenberg, H.; Covian, R.; Trumpower, B. L. *J. Biol. Chem.* **2009**, *284*, 19203−19210.

(16) Brand, M. D. *Exp. Gerontol.* **2010**, *45*, 466−472.

(17) Borek, A.; Sarewicz, M.; Osyczka, A. *Biochemistry* **2008**, *47*, 12365−12370.

(18) Sarewicz, M.; Borek, A.; Cieluch, E.; Świerczek, M.; Osyczka, A. *Biochim. Biophys. Acta, Bioenerg.* **2010**, *1797*, 1820−1827.

(19) Benov, L. *Protoplasma* **2001**, *217*, 33−36.

(20) Watts, R. J.; Washington, D.; Howsawkeng, J.; Loge, F. J.; Teel, A. L. *Adv. Environ. Res.* **2003**, *7*, 961−968.

(21) Harman, D. *J. Gerontol.* **1956**, *11*, 298−300.

(22) Ladiges, W.; Wanagat, J.; Preston, B.; Loeb, L.; Rabinovitch, P. *Aging Cell* **2010**, *9*, 462−465.

(23) Sastre, J.; Pallardó, F. V.; Viña, J. *IUBMB Life* **2000**, *49*, 427−435.

(24) Lenaz, G. *Biochim. Biophys. Acta, Bioenerg.* **1998**, *1366*, 53−67.

(25) Miquel, J. *Arch. Gerontol. Geriatr.* **1991**, *12*, 99−117.

(26) Linnane, A.; Ozawa, T.; Marzuki, S.; Tanaka, M. *Lancet* **1989**, *333*, 642−645.

(27) Cape, J. L.; Bowman, M. K.; Kramer, D. M. *Proc. Natl. Acad. Sci. U. S. A.* **2007**, *104*, 7887−7892.

(28) Jorgensen, W. L.; Chandrasekhar, J.; Madura, J. D.; Impey, R. W.; Klein, M. L. *J. Chem. Phys.* **1983**, *79*, 926−935.

(29) Phillips, J. C.; Braun, R.; Wang, W.; Gumbart, J.; Tajkhorshid, E.; Villa, E.; Chipot, C.; Skeel, R. D.; Kale, L.; Schulten, K. *J. Comput. Chem.* **2005**, *26*, 1781−1802.

(30) MacKerell, A. D.; Feig, M.; Brooks, C. L. *J. Comput. Chem.* **2004**, *25*, 1400−1415.

(31) Crofts, A. R.; Barquera, B.; Gennis, R. B.; Kuras, R.; Guergova-Kuras, M.; Berry, E. A. *Biochemistry* **1999**, *38*, 15807−15826.

(32) Postila, P. A.; Kaszuba, K.; Sarewicz, M.; Osyczka, A.; Vattulainen, I.; Róg, T. *Biochim. Biophys. Acta, Bioenerg.* **2013**, *1827*, 761−768.

(33) Kaszuba, K.; Postila, P. A.; Cramariuc, O.; Sarewicz, M.; Osyczka, A.; Vattulainen, I.; Róg, T. *Theor. Chem. Acc.* **2013**, *132*, 1−13.

(34) Frisch, M. J.; Trucks, G. W.; Schlegel, H. B.; Scuseria, G. E.; Robb, M. A.; Cheeseman, J. R.; Scalmani, G.; Barone, V.; Mennucci, B.; Petersson, G. A.; Nakatsuji, H.; Caricato, M.; Li, X.; Hratchian, H. P.; Izmaylov, A. F.; Bloino, J.; Zheng, G.; Sonnenberg, J. L.; Hada, M.; Ehara, M.; Toyota, K.; Fukuda, R.; Hasegawa, J.; Ishida, M.; Nakajima, T.; Honda, Y.; Kitao, O.; Nakai, H.; Vreven, T.; Montgomery, J. A., Jr.; Peralta, J. E.; Ogliaro, F.; Bearpark, M.; Heyd, J. J.; Brothers, E.; Kudin, K. N.; Staroverov, V. N.; Keith, T.; Kobayashi, R.; Normand, J.; Raghavachari, K.; Rendell, A.; Burant, J. C.; Iyengar, S. S.; Tomasi, J.; Cossi, M.; Rega, N.; Millam, J. M.; Klene, M.; Knox, J. E.; Cross, J. B.; Bakken, V.; Adamo, C.; Jaramillo, J.; Gomperts, R.; Stratmann, R. E.; Yazyev, O.; Austin, A. J.; Cammi, R.; Pomelli, C.; Ochterski, J. W.; Martin, R. L.; Morokuma, K.; Zakrzewski, V. G.; Voth, G. A.; Salvador, P.; Dannenberg, J. J.; Dapprich, S.; Daniels, A. D.; Farkas, O.; Foresman, J. B.; Ortiz, J. V.; Cioslowski, J.; Fox, D. J. *Gaussian 09*; Gaussian, Inc.: Wallingford, CT, 2013.

(35) Becke, A. D. *J. Chem. Phys.* **1993**, *98*, 5648−5652.

(36) Shoji, M.; Koizumi, K.; Kitagawa, Y.; Yamanaka, S.; Okumura, M.; Yamaguchi, K. *Int. J. Quantum Chem.* **2007**, *107*, 609−627.

(37) Bassan, A.; Blomberg, M. R.; Borowski, T.; Siegbahn, P. E. *J. Phys. Chem. B* **2004**, *108*, 13031−13041.

(38) Salomon, O.; Reiher, M.; Hess, B. A. *J. Chem. Phys.* **2002**, *117*, 4729−4737.

(39) Niu, S.; Nichols, J. A.; Ichiye, T. *J. Chem. Theory Comput.* **2009**, *5*, 1361−1368.

(40) Sigfridsson, E.; Olsson, M. H.; Ryde, U. *J. Phys. Chem. B* **2001**, *105*, 5546−5552.

(41) Wilkens, S. J.; Xia, B.; Weinhold, F.; Markley, J. L.; Westler, W. M. *J. Am. Chem. Soc.* **1998**, *120*, 4806−4814.

(42) Sigfridsson, E.; Olsson, M. H.; Ryde, U. *Inorg. Chem.* **2001**, *40*, 2509−2519.

(43) Szilagyi, R. K.; Winslow, M. A. *J. Comput. Chem.* **2006**, *27*, 1385−1397.

(44) Aguayo, D.; González-Nilo, F. D.; Chipot, C. *J. Chem. Theory Comput.* **2012**, *8*, 1765−1773.

(45) Gnaiger, E.; Lassnig, B.; Kuznetsov, A.; Rieger, G.; Margreiter, R. *J. Exp. Biol.* **1998**, *201*, 1129−1139.

(46) Darden, T.; York, D.; Pedersen, L. *J. Chem. Phys.* **1993**, *98*, 10089−10092.

(47) Allen, M. P.; Tildesley, D. J. *Computer Simulation of Liquids*; Oxford University Press: New York, 1989.

(48) Solov'yov, I. A.; Yakubovich, A. V.; Nikolaev, P. V.; Volkovets, I.; Solov'yov, A. V. *J. Comput. Chem.* **2012**, *33*, 2412−2439.

(49) Basconi, J. E.; Shirts, M. R. *J. Chem. Theory Comput.* **2013**, *9*, 2887−2899.

(50) Han, P.; Bartels, D. M. *J. Phys. Chem.* **1996**, *100*, 5597−5602.

(51) Windrem, D. A.; Plachy, W. Z. *Biochim. Biophys. Acta, Biomembr.* **1980**, *600*, 655−665.

(52) Cohen, J.; Kim, K.; King, P.; Seibert, M.; Schulten, K. *Structure* **2005**, *13*, 1321−1329.

(53) Şener, M.; Strümpfer, J.; Timney, J. A.; Freiberg, A.; Hunter, C. N.; Schulten, K. *Biophys. J.* **2010**, *99*, 67−75.

(54) Coombs, D.; Straube, R.; Ward, M. *SIAM J. Appl. Math.* **2009**, *70*, 302−332.

(55) Crofts, A. R.; Lhee, S.; Crofts, S. B.; Cheng, J.; Rose, S. *Biochim. Biophys. Acta, Bioenerg.* **2006**, *1757*, 1019−1034.

(56) Quinlan, C. L.; Gerencser, A. A.; Treberg, J. R.; Brand, M. D. *J. Biol. Chem.* **2011**, *286*, 31361−31372.

(57) Ksenzenko, M.; Konstantinov, A. A.; Khomutov, G. B.; Tikhonov, A. N.; Ruuge, E. K. *FEBS Lett.* **1983**, *155*, 19−24.

(58) Cape, J. L.; Bowman, M. K.; Kramer, D. M. *Trends Plant Sci.* **2006**, *11*, 46−55.

DOI: 10.1021/jacs.6b04849
J. Am. Chem. Soc. 2016, 138, 12150−12158

(59) Muller, F.; Crofts, A. R.; Kramer, D. M. *Biochemistry* **2002**, *41*, 7866−7874.

DOI: 10.1021/jacs.6b04849
J. Am. Chem. Soc. 2016, 138, 12150−12158